Analysis of the Multipath Effect of Human Presence on Indoor 60 GHz Wireless Channels

Bassel Abou Ali Modad*, Dajana Cassioli †, *Senior Member, IEEE*, and Andreas F. Molisch*, *Fellow, IEEE* *Dept. of Electrical and Computer Engineering, University of Southern California, Los Angeles, USA. {aboualim, molisch}@usc.edu

[†]Dept. of Information Engineering, Computer Science and Mathematics, University of L'Aquila, L'Aquila, Italy. dajana.cassioli@univaq.it

Abstract—The 60 GHz band plays an important role for wireless signalling with extremely high data rates, both for WiFi and cellular applications. For the design and performance analysis of this band, the impact of human interactions on the propagation from transmitter to receiver has to be taken into account. While the impact of a single human body blocking the line-of-sight (LOS) has been investigated as a deterministic effect, statistical models describing the effect of multiple human bodies, acting as reflectors, on received power and delay spread are still lacking. To close this gap, this paper analyzes measurements of 60 GHz channel impulse responses in static but "evolutionary" office scenarios that involve one and two people and uses them to calibrate a ray tracer that allows the generation of a larger number of channel realizations. Regression fits are applied to the resulting channel responses to obtain an accurate characterization of human-induced power and delay variations in proximity situations where humans give rise to additional multipath¹.

I. INTRODUCTION

Use of the millimeter-wave (mmWave) spectrum is an integral part of fifth generation (5G) wireless communications systems [1]. It enables very high data rates due to the availability of larger bandwidths compared to the traditional cellular and WiFi bands. Of particular interest is the 60 GHz band, in which 7 GHz of bandwidth are available for unlicensed operation (depending on the regulatory regime, up to 14 GHz might be available). Several wireless standards already use these bands, including the IEEE 802.11ad standard [2] and its more recent incarnation IEEE 802.11ay [3], which provide WiFi connectivity, i.e., short range high speed communications in indoor environments. Furthermore, while the 5G NR standard is currently only specified in frequency bands up to 51 GHz, its next release will include an expansion to up to 71 GHz. The 60 GHz band could then be used for either License Assisted Access (LAA), or stand-alone unlicensed access [4].

While there has been extensive work on the measurement and modeling of the wireless propagation channels in the 60 GHz band over the past 30 years (see, e.g., the reviews in [5], [6]), most of the work has been done in setups that avoided human presence in the measurement environment. Yet measuring and modeling the impact of human bodies is

essential as they can play a significant role as blockers or scatterers especially in indoor environments. For this reason, several papers have investigated the blockage of a line-of-sight (LOS) connection by a human body, e.g., [7]–[10] who measured the attenuation of the LOS component as a function of the position of the intervening human body. Similar measurements were performed in outdoor environments at 28 GHz in [11] and at 73 GHz in [12] and [13]. These results can be used for a deterministic modeling of such shadowing, as proposed in the 3GPP channel model [14].

A related but distinct avenue of investigation is the analysis of statistical channel variations in the presence of one or more human bodies. An early contribution to this topic was made by one of the authors of this paper [15]. Later works have employed both measurements and raytracing simulations to model the channel and the human effect [8], [16]. In particular, [16] studies the effect of one moving human on the delay spread, and [8] studies the signal coverage, LOS blockage duration and number of blockages per hour in the 60 GHz channel using several humans modelled as ellipses.

It is important to model not only the effect of one human, but multiple, since this is a more realistic scenario. To the best of our knowledge, such investigations are only done for the 60 GHz band in [8] and in our work [15]; however, the multipath effect was not studied. Additionally, none of the previous works study the impact of human presence on the statistical properties of channels such as delay spread, power distribution, number of multipath components (MPCs), MPCs inter-arrival times, and how they differ from the static case (with no humans). The only work that provides similar results, the recent paper [17], performed measurements in the 27 GHz band. This work carried out extensive indoor measurement campaigns with either a static or a moving receiver (RX) with different human obstructions. For the static RX case, two scenarios with one human blocker and six human blockers walking in random positions were carried out. Results showed that the multipath nature of the indoor environment limits blockage loss and delay spread changes. However, measurements were done in a different frequency band (27 vs. 60 GHz) and a different bandwidth (0.4 vs. 1.2 GHz) compared to the measurements used here. A qualitative comparison between the results in [17] and our results is done in Sec. V.

¹The work of B. Abou Ali Modad and A.F. Molsich was supported in part by the National Science Foundation and the National Institute of Standards and Technology.

To close this gap, this paper provides a statistical analysis of the multipath effect of human bodies on the 60 GHz channel in an indoor environment for the cases of one and two human bodies, and derives a statistical model. Since we have limited measurement results, we augment existing measurement results by raytracing, where the ray tracer is carefully calibrated against the measurement data. The augmented dataset is used for analysis of the delay spread, number of MPCs, the statistical distributions of the MPC powers and interarrival times in each case.

The remainder of the paper is organized as follows: in Section II, we present the measurement campaign. In Section III we discuss the augmentation using raytracer results. Section IV presents the results and analysis of the above-mentioned statistical parameters. Finally, Sec V concludes the paper and addresses future work.

II. CHANNEL MEASUREMENTS

A. Setup and Scenario

Fig. 1 shows the block diagram of the channel sounder. The transmitter (TX) is a pseudo-noise (PN) sequence channel sounder that creates an IF signal (4.2-5.4 GHz) with a bandwidth $B^{\rm IF}=1.2$ GHz [18]. This signal serves as input to an up-converter to the 60 GHz band described below. The resulting 60 GHz signal is sent through a power amplifier (PA) and is transmitted from a vertically polarized horn antenna with gain 25 dBi and beamwidth 9 degrees, mounted on a platform. The receiver (RX) antenna is omni-directional with a nominal gain of 2 dBi and vertical polarization. Both antennas are placed on the desks at a height of 0.97 m. The architecture of the down-converter is complementary to the up-converter. Passband filters are also added in the up- and down-converters for the 54-59 GHz and 61-66 GHz bands.

For the up/downconverter, the local oscillator (LO) chain is equipped with a tunable synthesizer (4 to 10 GHz), whose output is multiplied (in two steps) by a factor of 8, thus allowing the carrier frequency to span eight sub-bands of interest: four in the 54-59 GHz range, referred to as B_L and four in the 61-66 GHz range, referred to as B_H .

The LO feeds both the up- and down-converters. The output of the down-converter is the signal at the intermediate frequency $f_c^{\rm IF}=4.78$ GHz. It is amplified and sent to a digital sampling oscilloscope (DSO) that can display signals up to 6 GHz with a 20 GSps sampling frequency. The tuning of the synthesizer and the waveform acquisition by the DSO are software controlled. We refer the reader to [15] and [19] for further details.

The measurement environment is shown in Fig. 2. It is a typical office room bounded by a concrete wall with two windows, and plasterboard walls. There are several desks, a cabinet and one door on the wall opposite the windows. The TX and RX are marked by the black triangle and square, respectively, and are in fixed LOS positions for the entirety of the measurements (the LOS can be fully or partially obstructed during measurements). The TX antenna is properly

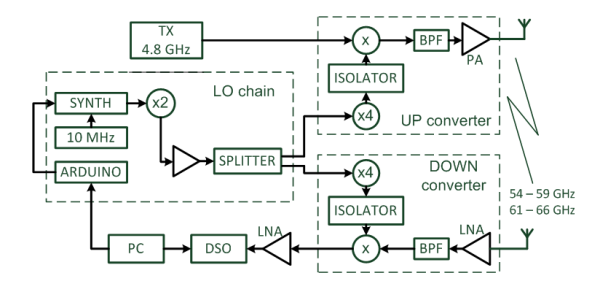


Fig. 1: Experimental setup.

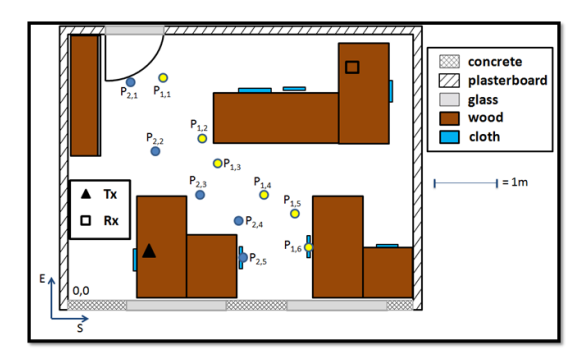


Fig. 2: Measurement scenarios.

oriented towards the RX antenna. A measurement in the room was made with no humans present; this serves as reference.

For reproducibility, the people involved remain in a fixed predefined position during the recording phase. In subsequent measurements, they move to another predefined position and the recording repeats. The positions are labeled in Fig. 2 as $P_{k,l}$ where k=1,2 is the person index, and l=1,...,6 is the location index. Additional positions were used in the campaign but are not related to the current study. For more details, we refer to the previous work in [15].

B. Post-processing

The probe signal is the periodic repetition of a PN-sequence with period 1023 chips. The recording of the received signal is done by the DSO using an observation window of 860 ns and a sampling time of 50 ps. The observation window is 40 ns longer than the nominal duration of the signal, to allow the complete decay of the channel impulse response (CIR) within that time. Coherent demodulation of the received signals is performed with a local carrier at a frequency of 4.78 GHz.

The CIRs are extracted through the CLEAN algorithm [20], a successive interference cancelation approach for deconvolution that estimates the arrival times and amplitudes of multipath components (MPCs). For further details, see [15].

The recovered measurements and estimated CLEAN arrival times are not synchronized in time with the start of the transmission. That is because the output power of the synchronization signal was too low to be detected by the DSO. Hence, we synchronize the measurements and CLEAN outputs by realigning the first peak of the measured power delay profiles (PDPs) and CLEAN outputs to the LOS path arrival time since the latter is always present (albeit partially

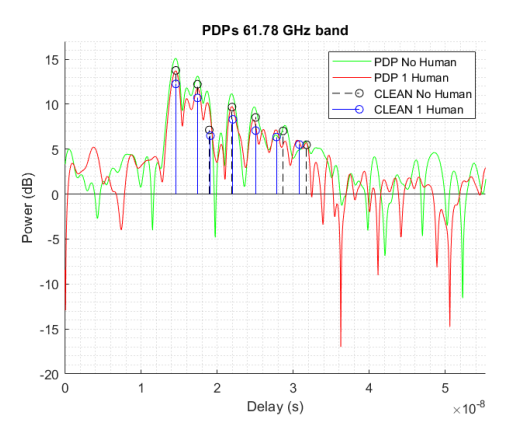


Fig. 3: PDPs and CLEAN output of measurements for the 61.78 GHz band for one-human at position $P_{1,3}$

obstructed). This allows better identification of MPCs and relating them to the geometry of the room.

III. RAYTRACER AUGMENTATION

To augment the existing measurements dataset, we developed a raytracer using MATLAB that simulates the measurement scenario and saves the resulting channel parameters (transmission angles, delays and powers of MPCs) for later statistical fitting.

The raytracer was calibrated using the existing measurement results (an example is shown in Fig. 3 where we compare the PDPs and estimated CLEAN paths for the empty room and in the presence of one human in the vicinity of the LOS) by iteratively changing the simulation parameters to account for particularities and non-idealities in the measurements. These are, e.g., material types of the obstacles, offsets in RX and TX positions, and orientation and beamwidth of the horn antenna. The calibration was done in the empty room so that the obtained raytracer PDPs are as close as possible to the experimental profiles. The raytracer was also calibrated on the cases with human presence near the LOS link $P_{1,3}$. The human position, shape and permittivity were iteratively changed to obtain the best agreement with the measurement profiles. We found that modeling the human as an ellipse, as in [21] and [8], with major axis length of 0.5 m and minor axis length of 0.3 m (as in [12]), and using skin permittivity ($\epsilon_r = 7.98 - 10.91j$ at 60 GHz [7]) gives the best agreement between profiles. Since the TX antenna is highly directional in the azimuth direction and is placed on top of the desk where it is above the furniture, no other desks and no furniture were included in the simulation, only the cabinet (labeled A in Fig. 2). We noticed in the measured PDPs a resonance of period 0.9 m due to a mismatch between the cables and the rest of the RF chain, which occurred because the measurements are from a previous campaign, described in [15], that studied shadowing and pathloss, which require only power calibration. This created additional ghost paths that are not present in the raytracer profiles and cannot be related to the geometry of the room. These periodic paths were ignored

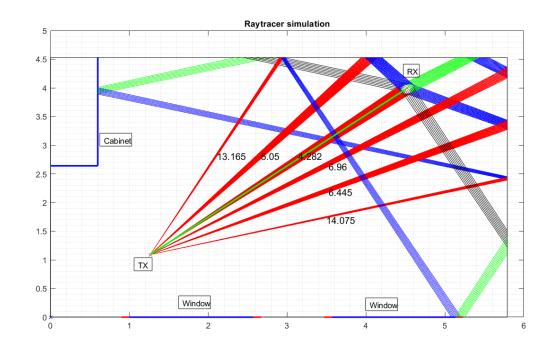


Fig. 4: Results of raytracing simulation in empty room.

Parameter	Value		
Launching beamwidth	30 degrees around LOS direction		
Human Orientation	60 degrees		
TX location	(1.265m, 1.0908m)		
RX location	(4.52m, 3.9928m)		
Human permittivity	7.98 - 10.91j (Skin [7])		
Upper wall permittivity	3.08 - 0.05544j (Plasterboard		
	[22])		
Lower wall permittivity	6.4954 - 0.4284j (Concrete [22])		
Right and left wall permittivities	2.4845 - 0.06211j (Plasterboard		
	5mm [22])		
Cabinet permittivity	6.3919 - 0.00032j (Glass [22])		

TABLE I: Raytracer simulation parameters

when calibrating the raytracer and only the paths that can be related to the geometry were used for the calibration.

The raytracer launches rays in a specific beamwidth around the LOS link, computes intersections and reflections of rays from the obstacles in the environment (walls, windows, closet) and the resulting reflection coefficients as [22]

$$\rho_0 = \frac{\cos \theta_0 - \sqrt{\epsilon_r - \sin^2 \theta_0}}{\cos \theta_0 + \sqrt{\epsilon_r - \sin^2 \theta_0}} \tag{1}$$

where θ_0 is the angle between the incident and reflected rays, and ϵ_r is the relative permittivity of the obstacle at 60 GHz. Launched powers of the rays need to be attenuated according to the antenna gain pattern. Since this pattern was not provided with the data sheet of the horn antenna, we tried to fit measurement results with various shapes; we found that a step-wise 3 dB decrease in power every 9° on both sides of the LOS link, and assuming the power to be 0 outside the launch beamwidth, gives the best agreement between profiles. Free space path-loss and gains of all components in the RF chain were taken into account as well. Note that according to [10], diffraction can be neglected at 60 GHz almost everywhere in a room except in a small region of a few centimeters around the shadow boundary, so we can safely ignore diffraction. We use a reception sphere around the receiver of radius 0.1 m to collect the rays that are incident around the omni-directional antenna. The simulation parameters are shown in Table I and a visualization of the rays is shown in Fig. 4 with the ray lengths overlayed.

The rays were reflected three times as we found it to be sufficient for accurate results; each bounce is symbolized by

Number of humans	Distribution
One-human	Normal $\mathcal{N}(\mu = 5.56, \sigma^2 = 7.86)$
Two-human	Normal $\mathcal{N}(\mu = 5.83, \sigma^2 = 8.64)$

TABLE II: Best fits of the number of MPCs due to human presence for one- and two-humans

a different color in Fig. 4. After calibration, we simulate 500 different uniformly distributed random positions for the one-human case and the two-humans case respectively, as we only have measurements for two moving humans to compare to. A higher number of humans will be part of future work.

IV. RESULTS AND ANALYSIS

We analyze the interarrival times, power statistics, rootmean-square (RMS) delay spread, and number of additional MPCs created by the humans. The below analysis is based on the ensemble of 500 simulations for each number of humans.

For the interarrival times, we specifically select the MPCs that have been reflected by the humans. It is important to distinguish between rays and clusters. Most MPCs arrive in clusters with small intra-cluster separations, this causes a peak in the interarrival times distribution around very small values. However, the MPCs inside each cluster may not always be resolved by a system depending on the bandwidth used; in other words the finite bandwidth results in "binning" of the delays into groups, where the size of a bin is the inverse of the bandwidth.

The interarrival time distributions resulting from a 10 GHz bandwidth filter are shown in Fig. 5 for one- and two-humans, respectively, with the best fit distributions. The interarrival times are fitted to the exponential distribution and show a good agreement, which confirms the assumption of Poisson arrivals of MPCs. The decay time constant is $2.38 \cdot 10^8 \ s^{-1}$ for the one-human case. Note that tighter filtering will lead to a (slightly) slower decay constant, reaching $2.09 \cdot 10^8 \ s^{-1}$ for 2.1 GHz bandwidth (the narrowest bandwidth for 802.11ad systems).

The decay constant of the fitted exponential distribution for the two-humans case is $2.46 \cdot 10^8 \ \mathrm{s^{-1}}$ for a 10 GHz bandwidth, indicating a shorter interarrival time between MPCs on average for two-humans. This is in line with the intuition that a richer multipath environment arises due to the additional human. This is also confirmed by the distribution of the number of MPCs generated by human presence, with a 10 GHz bandwidth filter, for one- and two-humans in Fig. 6 and Table II. We can see that generally the two-humans case leads to a higher probability of a large number of MPCs, and to a higher variance. The best fit distributions for both cases are (truncated) normal distributions shown in Fig. 6 and Table II. Note that the estimated normal distributions should be truncated to keep only the positive values when used in simulations.

As for the RMS delay spread, its cumulative distribution function (CDF) for the one- and two-humans cases is shown in Fig. 7. We notice that the distributions are similar, which is in line with the results of [17] for the 27 GHz band. The

Parameter	1^{st} region	2^{nd} region	3^{rd} region	4 th region
a	$4.889 \cdot 10^5$	1761.879	-0.106	31.506
b	$2.892 \cdot 10^{6}$	-6.744·10 ⁸	-1.398·10 ⁸	-3.647·10 ⁸
c	-4.889·10 ⁵	$4.78 \cdot 10^{12}$	0.288	$6.519 \cdot 10^{-4}$
d	$2.892 \cdot 10^{6}$	-1.95·10 ⁹	-1.551·10 ⁸	$-9.472 \cdot 10^7$

TABLE III: Mean decay two-term exponential fitting results

delay spread for the static channel with no human present is 7.5 ns, which corresponds to the mean of the distributions in Fig. 7.

To model the powers of the human generated MPCs, we proceed in two steps: (i) modeling the average decay of the powers over the ensemble of PDPs and (ii) modeling the deviations from that average. This is in line with how to use the resulting models to generate channel realizations for simulation purposes.

First, we group the individual PDP realizations of each simulation run into one "ensemble PDP". Note that this is not a "PDP" per se, since a PDP requires the wide sense stationary - uncorrelated scattering (WSSUS) assumptions to be satisfied, which is not the case here: WSSUS requires, among other conditions, that the powers in the individual contributions are constant and at the same delays for different realizations, which is often violated for large-bandwidth channels, including the ones here. However, we will use the term "ensemble PDP" as the average of the PDPs, for the purpose of analysis of the channel properties over all realizations. For a more detailed discussion of these aspects, we refer to [23].

The resulting ensemble PDP is shown in Fig. 8. We notice similar regions of distinct behavior in the ensemble PDPs for both one- and two-humans. The first region is a deterministically decaying one where the delays correspond to distances between 4.38 m and 5.16 m, which are MPCs due to reflections when the humans are close to the LOS link, hence the small additional delay (recall that the LOS link is 4.36 m long). We fit this part to a two-term exponential function of the form $ae^{bx} + ce^{dx}$, as this provides a better fit than a one-term exponential. The rest of the PDPs follow a decay with visible clusters (peaks in Fig. 8) each of which we analyze separately for better accuracy. We identify three regions associated with the three visible clusters and they are denoted in Fig. 8. We fit the decay of each cluster to the same two-term exponential function. The resulting parameters for all regions are shown in Table III.

To model the deviations from this mean decay, we only use the part after the deterministic first region, as this part shows the variations. The empirical CDF of these deviations for one- and two-humans is best fitted with a normal CDF on a dB scale, hence a lognormal CDF on a linear scale. The mean and standard deviation of the normal distribution for the one-human case are 1.96 dB and 4.78 dB respectively, and 1.45 dB and 4.47 dB respectively for the two-humans case. Both cases are shown in Fig. 9 on a dB scale.

Note that the similarity between the one- and two-human cases in all the results is due to the small space in which the humans can be placed, the orientation of the humans and

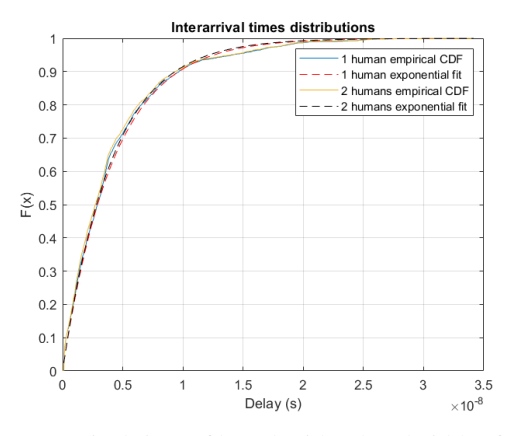


Fig. 5: Interarrival times filtered with a bandwidth of 10 GHz and corresponding exponential fits for one- and two-humans

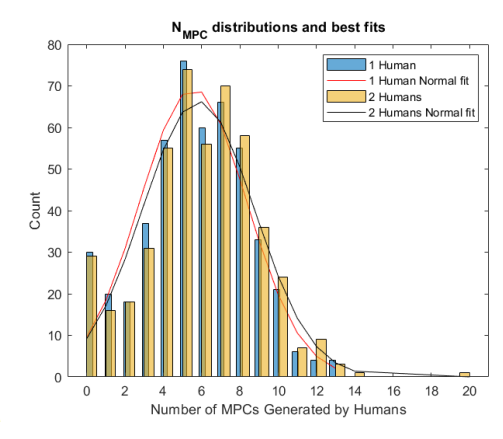


Fig. 6: Number of MPCs due to human presence for one- and two-humans and their respective best fit normal distributions

the beamwidth of the launched rays. There are only specific positions where the angles of reflection from the humans reach the RX while obeying Snell's law for this particular orientation, and one human's position can be outside of the launch beamwidth while the other can be inside, potentially leading to reflections that reach the RX. Finally, we show how our models can be used to generate channel realizations in the flowchart of Fig. 10

V. CONCLUSION

In this work, we studied the effect of human presence for one and two humans on the indoor multipath channel at 60 GHz. The analysis is based on real measurements that were used to calibrate a raytracer and generate an extended dataset to investigate. We validated the hypothesis that for the 60 GHz band, MPCs are generated according to a Poisson process (exponentially distributed interarrival times) in the presence of humans. No significant change occurs in the delay spread when an additional human is present, similarly to the literature on the 27 GHz band. Powers of the MPCs follow an exponential decay on average with deviations that can be modeled by a lognormal distribution in the linear scale. Future work will include conducting new measurement campaigns,

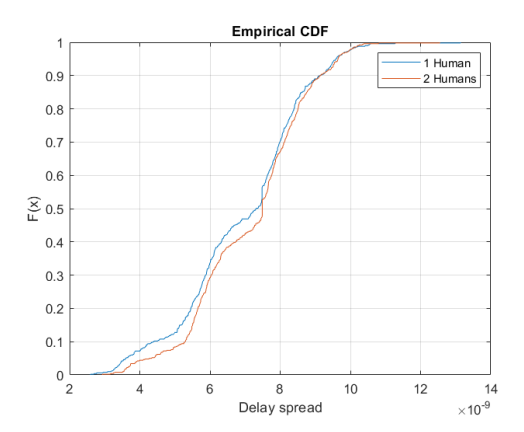
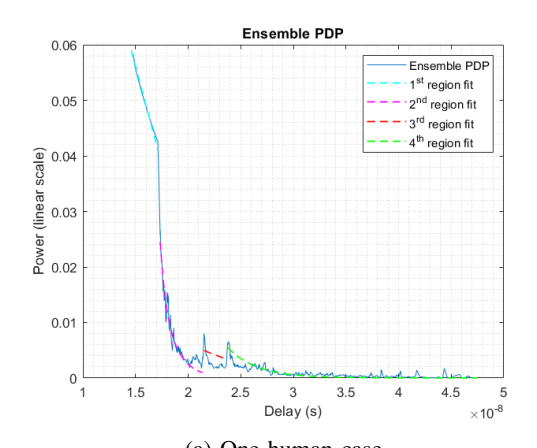


Fig. 7: Delay Spread CDF for one- and two-humans



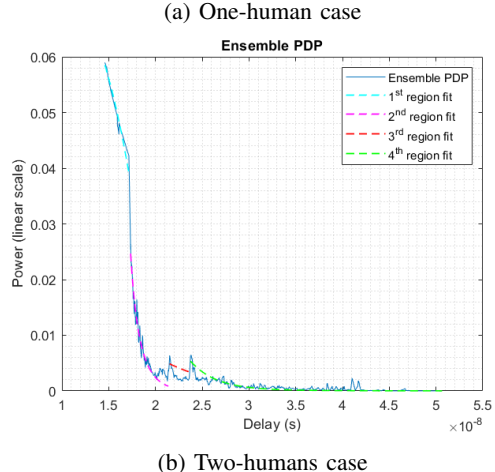


Fig. 8: Ensemble PDP with 10 GHz bandwidth filtering and fits for each cluster region for (a) one-human and (b) two-humans

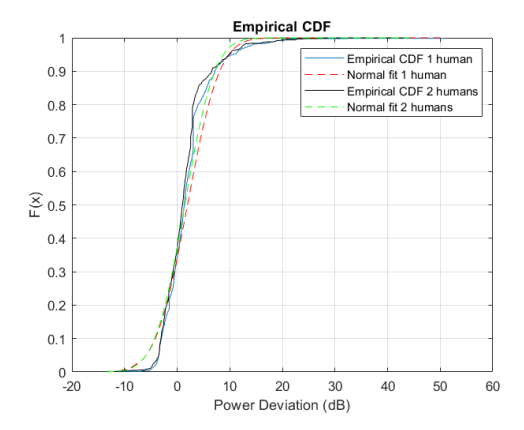


Fig. 9: CDF of the power deviations in dB and the corresponding normal fits for one- and two-humans

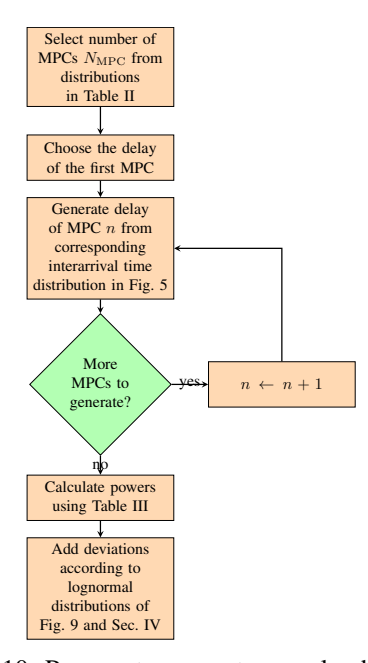


Fig. 10: Process to generate sample channel

simulation of more than two humans, and modeling the differential effect that each human produces on the multipath channel.

REFERENCES

- [1] M. Shafi, A. F. Molisch, P. J. Smith, T. Haustein, P. Zhu, P. De Silva, F. Tufvesson, A. Benjebbour, and G. Wunder, "5G: A tutorial overview of standards, trials, challenges, deployment, and practice," *IEEE Jour*nal on Selected Areas in Communications, vol. 35, no. 6, pp. 1201– 1221, 2017.
- [2] "IEEE standard for information technology-telecommunications and information exchange between systems-local and metropolitan area networks-specific requirements-part 11: Wireless lan medium access control (mac) and physical layer (phy) specifications amendment 3: Enhancements for very high throughput in the 60 GHz band," IEEE Std 802.11ad-2012 (Amendment to IEEE Std 802.11-2012, as amended by IEEE Std 802.11ae-2012 and IEEE Std 802.11aa-2012), pp. 1-628, 2012.
- [3] "IEEE standard for information technology-telecommunications and information exchange between systems local and metropolitan area networks-specific requirements part 11: Wireless lan medium access

- control (mac) and physical layer (phy) specifications amendment 2: Enhanced throughput for operation in license-exempt bands above 45 GHz," *IEEE Std 802.11ay-2021 (Amendment to IEEE Std 802.11-2020 as amendment by IEEE Std 802.11ax-2021)*, pp. 1–768, 2021.
- [4] E. Dahlman, S. Parkvall, and J. Sköld, "Chapter 5 nr overview," in 5G NR: the Next Generation Wireless Access Technology, E. Dahlman, S. Parkvall, and J. Sköld, Eds. Academic Press, 2018, pp. 57–71. [Online]. Available: https://www.sciencedirect.com/science/article/pii/B9780128143230000053
- [5] P. Smulders, "Exploiting the 60 GHz band for local wireless multimedia access: prospects and future directions," *IEEE Communications Magazine*, vol. 40, no. 1, pp. 140–147, 2002.
- [6] A. F. Molisch, T. Choi, N. Abbasi, F. Rottenberg, and J. Zhang, "Millimeter-wave channels," Wiley 5G Ref: The Essential 5G Reference Online, pp. 1–46, 2019.
- [7] C. Gustafson and F. Tufvesson, "Characterization of 60 ghz shadowing by human bodies and simple phantoms," in 2012 6th European Conference on Antennas and Propagation (EUCAP), 2012, pp. 473–477.
- [8] B. Peng, S. Rey, D. M. Rose, S. Hahn, and T. Kuerner, "Statistical characteristics study of human blockage effect in future indoor millimeter and sub-millimeter wave wireless communications," in 2018 IEEE 87th Vehicular Technology Conference (VTC Spring), 2018, pp. 1–5.
- [9] L. Ahumada Fierro, E. C. Maggi, A. Anglès Vazquez, and D. Schkolnik, "Empirical results for human-induced shadowing events for indoor 60 GHz wireless links," *IEEE Access*, vol. 8, pp. 44 522–44 533, 2020.
- [10] M. Jacob, S. Priebe, R. Dickhoff, T. Kleine-Ostmann, T. Schrader, and T. Kurner, "Diffraction in mm and sub-mm wave indoor propagation channels," *IEEE Transactions on Microwave Theory and Techniques*, vol. 60, no. 3, pp. 833–844, 2012.
- [11] T. Choi, C. U. Bas, R. Wang, S. Hur, J. Park, J. Zhang, and A. F. Molisch, "Measurement based directional modeling of dynamic human body shadowing at 28 GHz," in 2018 IEEE Global Communications Conference (GLOBECOM), 2018, pp. 1–6.
- [12] G. R. MacCartney, S. Deng, S. Sun, and T. S. Rappaport, "Millimeter-wave human blockage at 73 GHz with a simple double knife-edge diffraction model and extension for directional antennas," in 2016 IEEE 84th Vehicular Technology Conference (VTC-Fall), 2016, pp. 1–6.
- [13] G. R. MacCartney, T. S. Rappaport, and S. Rangan, "Rapid fading due to human blockage in pedestrian crowds at 5G millimeter-wave frequencies," in GLOBECOM 2017 - 2017 IEEE Global Communications Conference, 2017, pp. 1–7.
- [14] 3GPP, "TR 38.901 v17.0.0 study on channel model for frequencies from 0.5 to 100 GHz (release 17)," 2022.
- [15] D. Cassioli and N. Rendevski, "A statistical model for the shadowing induced by human bodies in the proximity of a mmwaves radio link," in 2014 IEEE International Conference on Communications Workshops (ICC), 2014, pp. 14–19.
- [16] M. Jacob, S. Priebe, A. Maltsev, A. Lomayev, V. Erceg, and T. Kürner, "A ray tracing based stochastic human blockage model for the IEEE 802.11ad 60 GHz channel model," in *Proceedings of the 5th European Conference on Antennas and Propagation (EUCAP)*, 2011, pp. 3084–2089
- [17] R. Schulpen, L. Bronckers, A. Smolders, and U. Johannsen, "Impact of human blockage on dynamic indoor multipath channels at 27 ghz," *IEEE Transactions on Antennas and Propagation*, pp. 1–1, 2022.
- [18] W. Ciccognani, A. Durantini, and D. Cassioli, "Time Domain Propagation Measurements of the UWB Indoor Channel using PN–Sequence in the FCC–Compliant Band 3.6-6 GHz," *IEEE Trans. on Ant. and Prop.*, Apr. 2005.
- [19] S. Piersanti, L. A. Annoni, and D. Cassioli, "Millimeter waves channel measurements and path loss models," in *IEEE ICC 2012*, Jun. 2012.
- [20] J. A. Högbom, "Aperture Synthesis with a Non-Regular Distribution of Interferometer Baselines,", vol. 15, p. 417, Jun. 1974.
- [21] T. S. Rappaport, K. A. Remley, C. Gentile, A. F. Molisch, and A. Zajic, Radio Propagation Measurements and Channel Modeling. Cambridge Univ Press, 2022.
- [22] Y. Pinhasi, A. Yahalom, and S. Petnev, "Propagation of ultra wideband signals in lossy dispersive media," in 2008 IEEE International Conference on Microwaves, Communications, Antennas and Electronic Systems, 2008, pp. 1–10.
- [23] A. Meijerink and A. F. Molisch, "On the physical interpretation of the saleh-valenzuela model and the definition of its power delay profiles," *IEEE Transactions on Antennas and Propagation*, vol. 62, no. 9, pp. 4780–4793, 2014.

Correction to: "Analysis of the Multipath Effect of Human Presence on Indoor 60 GHz Wireless Channels" published in ICC 2023-IEEE International Conference on Communications

Correction submitted by: Dajana Cassioli and Andreas F. Molisch

Date correction submitted: July 2, 2024

DOI of original article: 10.1109/ICC45041.2023.10278884

Correction

In Sec. II.A the paper states the following paragraph: "The resulting 60 GHz signal is sent through a power amplifier (PA) and is transmitted from a vertically polarized horn antenna with gain 25 dBi and beamwidth 9 degrees, mounted on a platform."

However, the following text (bold) clarifies better the measurement setup characteristics: "... mounted on a platform and turned of 90 degrees around the axis corresponding to the main lobe of its radiation pattern resulting in a horizontal polarization of the emitted radiation. This way the collected measurements show the cross-polarization components detected by the receiving, vertically polarized antenna."